NASA TECHNICAL NOTE

NASA TN D-7833

NASA TN D-7833

(NASA-TN-D-7833) COMPARISON OF THREE METHODS FOR CALCULATION OF HELICOPTER ROTOR BLADE LOADING AND STRESSES DUE TO STALL (NASA) 25 p HC $3.25 CSCL 01B

N75-10935

Unclas
H1/05 02910

COMPARISON OF THREE METHODS FOR CALCULATION OF HELICOPTER ROTOR BLADE LOADING AND STRESSES DUE TO STALL

by Wayne Johnson

Ames Research Center

and

U.S. Army Air Mobility R&D Laboratory

Moffett Field, Calif. 94035

NATIONAL AERONAUTICS AND SPACE ADMINISTRATION • WASHINGTON, D. C. • NOVEMBER 1974

1. Report No.	2. Government Accession No.	3. Recipient's Catalog No.
D-7833		

4. Title and Subtitle	5. Report Date
COMPARISON OF THREE METHODS FOR CALCULATION OF HELICOPTER ROTOR BLADE LOADING AND STRESSES DUE TO STALL	November 1974
	6. Performing Organization Code
7. Author(s)	8. Performing Organization Report No.
Wayne Johnson	A-5337
	10. Work Unit No.
	760-63-02
9. Performing Organization Name and Address	11. Contract or Grant No.
Ames Research Center, NASA and U.S. Army Air Mobility R&D Laboratory Moffett Field, Calif. 94035	
	13. Type of Report and Period Covered
12. Sponsoring Agency Name and Address	Technical Note
National Aeronautics and Space Administration Washington, D. C. 20546	14. Sponsoring Agency Code

15. Supplementary Notes

16. Abstract

A comparison is made of the results of three methods for calculating the effects of dynamic stall on the performance, airloads, and blade stresses of a helicopter rotor at high loading. The three dynamic-stall methods considered predict essentially the same performance and trim for the rotor. They give roughly the same mean bending moments, but the peak-to-peak torsion and bending moments differ by 25 to 40 percent, and there are differences in the details of the predicted blade motion and stresses. The latter are due to significant differences in the dynamic stall aerodynamic loads, particularly the aerodynamic pitch moment, predicted by the three methods.

17. Key Words (Suggested by Author(s))	18. Distribution Statement
Helicopter rotor loads Unsteady stall Stall	Unclassified – Unlimited CAT.02

19. Security Classif. (of this report)	20. Security Classif. (of this page)	21. No. of Pages	22. Price*
Unclassified	Unclassified	21	$3.00

*For sale by the National Technical Information Service, Springfield, Virginia 22151

NOMENCLATURE

A_{1s}	lateral cyclic pitch, deg
B_{1s}	longitudinal cyclic pitch, deg
c_d	blade section drag coefficient
c_ℓ	blade section lift coefficient
c_m	blade section moment coefficient
C_Q	$Q/\rho\,(\Omega R)^2 \pi R^3$
C_T	$T/\rho\,(\Omega R)^2 \pi R^2$
C_X	$PF/\rho\,(\Omega R)^2 \pi R^2$
f	rotor equivalent parasite drag area, m^2
L	lift force
M	moment; Mach number
M_{pitch}	moment about blade feathering axis, N-m
M_x	rotor roll moment, N-m
M_y	rotor pitch moment, N-m
P	rotor power, hp
PF	rotor propulsive force, N
Q	rotor torque, N-m
r	rotor blade radial station ($r = 0$ at center of rotation, $r = R$ at tip)
R	rotor radius
T	rotor thrust, N
Y	rotor side force, N
α	blade section angle of attack, deg
β_o	rotor coning angle, deg

β_{1C}	cyclic flap, pitch (forward) of tip path plane, deg
β_{1S}	cyclic flap, roll (to left) of tip path plane, deg
ζ_O	mean blade lag angle, deg
θ_e	elastic torsion
$\theta_{.75}$	rotor collective pitch angle (at $r/R = 0.75$), deg
λ_{TPP}	rotor inflow velocity (divided by tip speed), in the tip path plane
μ	rotor advance ratio: helicopter forward speed divided by rotor tip speed
ρ	air density
σ	rotor solidity: ratio of total blade area to rotor disk area
ψ	rotor blade azimuth angle, measured from downstream direction
Ω	rotor rotational speed
$(\dot{})$	time derivative

COMPARISON OF THREE METHODS FOR CALCULATION OF HELICOPTER ROTOR BLADE LOADING AND STRESSES DUE TO STALL

Wayne Johnson

Ames Research Center
and
U. S. Army Air Mobility R&D Laboratory

SUMMARY

A comparison is made of the results of three methods for calculating the effects of dynamic stall on the performance, airloads, and blade stresses of a helicopter rotor at high loading. The three dynamic-stall methods considered predict essentially the same performance and trim for the rotor. They give roughly the same mean bending moments, but the peak-to-peak torsion and bending moments differ by 25 to 40 percent, and there are differences in the details of the predicted blade motion and stresses. The latter are due to significant differences in the dynamic stall aerodynamic loads, particularly the aerodynamic pitch moment, predicted by the three methods.

INTRODUCTION

Rotor blade stall usually is the limiting factor in helicopter maneuver and high-speed capability. Particularly important are the vibration and control system loads due to the high transient lift force and pitching moment of the periodically stalling blade. An adequate theoretical model of the stall process is therefore required for accurate design of the helicopter and prediction of its performance and limitations. Prediction of the aerodynamic loads of the stalled rotor blade is complicated, however, by the complex aerodynamic environment in which the blade operates. Rotor blade stall is always an unsteady and three-dimensional phenomenon, so it is not sufficient to use static, two-dimensional airfoil section data.

Considerable theoretical and experimental research has been conducted into the nature of unsteady, or dynamic, stall. Based on this research, several semi-empirical methods have been developed to incorporate the effects of dynamic stall into the calculation of the performance, airloads, and blade stresses of the helicopter rotor at high loading.

This report compares the results of three such methods, which are described briefly below. Additional details are provided in appendix A and the references cited.

1. UARL Method (refs. 1,2). Tabular data for c_ℓ and c_m as a function of α, $\dot{\alpha}$, and $\ddot{\alpha}$ are used to calculate the stall loads. These data were synthesized from oscillating airfoil test results. Static airfoil data are used below the stall angle of attack.

2. MIT Method (refs. 3–5). High transient c_ℓ and nosedown c_m are used at the occurrence of dynamic stall. The dynamic stall loading is basically impulsive, and then static stall values are used. The peak c_ℓ and c_m, as a function of $\dot{\alpha}$, are based on the experimental results of reference 3. Static airfoil data are used below the stall angle of attack.

3. Boeing Method (refs. 6,7). The actual angle of attack is corrected as a function of $\dot{\alpha}$ to obtain an effective angle α_{dyn}. Then c_ℓ, c_d, and c_m are obtained from static airfoil data using α_{dyn}. The angle-of-attack correction is based on oscillating airfoil test results.

CALCULATION CASES

The stall methods were compared by calculating the rotor performance and blade loads at a high speed, high thrust ($\mu = 0.333$, $C_T/\sigma = 0.09$) operating condition. Appendix B gives the details of the rotor operating state; the geometrical, inertial, structural, and aerodynamic characteristics of the rotor blade; and the parameters involved in the calculation process. These rotor and operating condition parameters were developed by Ormiston (ref. 8), for a general comparison of several methods of predicting the loads on a hypothetical rotor. The rotor performance and loads were calculated using a computer program based on reference 9, and incorporating the three stall methods considered here. Hence, the only difference in the methods is in the calculation of c_ℓ, c_d, and c_m for the blade sections, and this difference is apparent mainly at high angle of attack since all three methods use the same static airfoil data for low angle of attack. The following cases were considered:

CASE 1: Linear, incompressible aerodynamics ($c_\ell = 5.7\alpha$, $c_d = 0.0086$, $c_m = 0$); in other words, no stall. This base case is also used to examine the influence of nonuniform inflow (Case 1A, uniform inflow) and the influence of elastic blade motion (Case 1B, which uses only rigid flap and lag modes, as well as uniform inflow).

CASE 2: Static stall; static airfoil data used for all α

CASE 3: UARL stall method.

CASE 4. MIT stall method.

CASE 5: Boeing stall method.

Static airfoil data for an NACA 0012 section, in tabular form, were used in all three methods for the loads below stall. All the cases (except 1A and 1B) used nonuniform inflow, which was calculated by a separate program. Hence, the inflow distribution was prescribed in these calculations, and was the same for every case.

RESULTS AND DISCUSSION

Figure 1 shows the nonuniform inflow distribution used in the calculations. The role of the inflow distribution is indicated in figures 2 and 3, which are polar plots of the angle-of-attack

distribution over the rotor disk for cases 1A and 1, respectively. Case 1A uses uniform inflow and case 1 the nonuniform inflow; neither includes stall aerodynamics or the effect of the blade motion due to stall.

Table 1 presents the performance and trim data calculated for the seven cases considered. Cases 1, 1A, and 1B are with no stall; cases 1A and 1B examine the influence of uniform inflow and rigid blade motion, respectively. Case 2 uses static stall. Compared with the no-stall and the dynamic-stall cases, the static stall case shows very high values for power required, rotor flapping, and control angles (collective and cyclic), even though the thrust is still somewhat below the target value. These results imply that this operating condition (the combination of thrust, propulsive force, and forward speed) would be beyond the capability of this rotor if the blade stalled statically. The loads and the bending and torsion moments calculated for case 2 are unrealistic, therefore, and are not included in the other comparisons presented here. The three dynamic stall methods (cases 3, 4, and 5) give essentially the same results for performance and trim. Comparing, for example, the power required for these three cases with that for the no-stall case, it is evident that the stall effects are quite important. However, the effects predicted using the dynamic-stall models are much less than those obtained using static-stall data (case 2).

Table 1 also presents the results for the vertical and inplane root shear forces of the rotor. Only the harmonics transmitted to the helicopter body are given. There is a trend to increased magnitude of the higher harmonics due to stall. The variation of the root shear forces between the cases is an indication of the general sensitivity of the problem of calculating helicopter rotor vibration, as well as the difference between the stall models.

Figure 4 compares the elastic torsion motion of the blade, for the three dynamic stall methods. Since only one mode is used to represent the torsion motion, the torsion moments are directly proportional to the torsion deflection. Figure 4 shows significant differences in the details of the torsion moment waveform, particularly on the retreating side where dynamic stall is involved. The peak-to-peak torsion moments given by the three methods differ by about 40 percent. Figures 5 through 8 show the peak-to-peak and mean flatwise and edgewise blade bending moments for the three dynamic stall cases and the no-stall results (case 1). The mean bending moments predicted by the three stall cases are roughly the same. The higher mean edgewise moment compared with the no-stall case is due to the increased blade section drag associated with stall. Consequently the increase in the edgewise bending moment is about the same as the increase in the power required. The calculated peak-to-peak bending moments show roughly the same general characteristics, but the magnitude predicted by the three stall methods differ by about 25 to 40 percent.

The differences in the calculated blade torsion and bending moments may be traced to the blade aerodynamic loading. Figures 9 to 12 present the section lift force, and figures 13 to 16 the section pitching moment for the no-stall case (case 1) and the three dynamic-stall methods (cases 3, 4, and 5). There are significant differences in the aerodynamic loading, particularly in the pitch moment, due to the fundamental differences in the calculation of the dynamic stall loads in the three methods.

CONCLUDING REMARKS

The three dynamic-stall methods considered predict essentially the same performance and trim for the rotor. They give roughly the same mean bending moments, but the peak-to-peak torsion and bending moments differ by 25 to 40 percent, and there are differences in the details of the predicted blade motion and stresses. The latter are due to significant differences in the dynamic-stall aerodynamic loads, particularly the aerodynamic pitch moment, predicted by the three methods. The semi-empirical methods that have been developed to incorporate dynamic-stall effects into helicopter airloads calculations are useful and important advances. However, the fundamental differences in the aerodynamic loads predicted by the various methods suggest a need for further study into the fundamentals of the aerodynamic problem before a fully confident prediction of all helicopter rotor stall effects is possible.

Ames Research Center, NASA
and
U.S. Army Air Mobility R&D Laboratory
Moffett Field, Calif. 94035, July 10, 1974

APPENDIX A

THREE METHODS OF CALCULATING DYNAMIC STALL EFFECTS

UARL Method

The UARL method calculating dynamic stall airloads is based on data from tests of a NACA 0012 airfoil oscillating in pitch. The data for lift and moment coefficients c_ℓ and c_m are correlated as a function of α, $A = \dot{\alpha}c/2V$, and $B = \ddot{\alpha}(c/2V)^2$, by cross-plotting the oscillating airfoil data. The stall method uses these data for c_ℓ and c_m as a function of α, A, and B. The data are given in tabular form in reference 2. Figure 17 presents typical results for c_ℓ and c_m as a function of α, for several values of $\dot{\alpha}$ and with $\ddot{\alpha} = 0$. Compressibility effects are accounted for by scaling the incompressible data for c_ℓ and c_m.

MIT Stall Method

The MIT stall method is a theoretical model of the dynamic-stall loading of an airfoil for the calculation of helicopter airloads and blade motion. It is based on the experimental data of reference 3 for the peak transient airfoil loads during dynamic stall. When the angle of attack reaches the dynamic-stall angle α_{Ds} (which is above the static-stall angle α_{ss}), dynamic stall of the section occurs, resulting in a sharp increase in the lift and nosedown moment. The peak c_ℓ and c_m are functions of $\dot{\alpha}c/V$ at the instant of stall. The rise time of the loads to the peak values, and the fall time to static stall is small. Hence, the model involves essentially impulsive loading of the blade occurring at dynamic stall, with maximum loads $c_{\ell_{max}}$ and $c_{m_{max}}$, after which the blade has static-stall loads until the flow reattaches (reattachment is assumed to occur at the static stall angle α_{ss}).

When the blade section angle of attack exceeds α_{OS}, dynamic stall occurs at that section, producing high transient loads. From reference 3, the c_ℓ and c_m at stall are:

$$c_{\ell_{max}} = \begin{cases} 1 + 40|\dot{\alpha}c/V| & \dot{\alpha}c/V < 0.05 \\ 3 & \dot{\alpha}c/V > 0.05 \end{cases}$$

$$c_{m_{max}} = \begin{cases} -0.15 & \dot{\alpha}c/V < 0.02 \\ 0.283 - 21.7|\dot{\alpha}c/V| & 0.02 < \dot{\alpha}c/V < 0.05 \\ -0.80 & \dot{\alpha}c/V > 0.05 \end{cases}$$

A linear rise of the lift and moment to the peak values, in time $\Delta\psi_{RT}$, is used. Then a linear decay to static stall c_ℓ and c_m occurs. When the transient dynamic-stall loads have decayed, c_ℓ and c_m are assumed to take the static-stall values. For the NACA 0012 airfoil, best correlation is obtained with $\alpha_{Ds} = 15°$, $\Delta\psi_{RT} = 10°$ and $\alpha_{ss} = 12°$ (for reattachment).

Boeing Stall Method

The Boeing stall method is a theoretical model for the unsteady aerodynamics of a blade section, including dynamic-stall and radial flow effects. It is based on static airfoil data (c_ℓ, c_m, and c_d as function of α and M), with the angle of attack corrected for unsteady aerodynamics:

$$c_\ell = \min \left\{ \frac{c_\ell(\alpha_{\mathrm{dyn},L})}{\alpha_{\mathrm{dyn},L} \cos \Lambda}, \quad c_{\ell_\alpha} \right\} \alpha_{\mathrm{equ}}$$

$$c_m = c_m(\alpha_{\mathrm{dyn},M}) - \frac{\pi}{2} \frac{c}{V} (\beta + \dot{\theta})$$

$$c_d = c_d(\alpha_{\mathrm{dyn},M}) + c_{d_{SF}} \left(\frac{1}{\cos \Lambda} - 1 \right)$$

where Λ is the sweep angle, and $c_{d_{SF}}$ is the skin friction drag coefficient. The correction for the effect of sweep on the lift is just (ignoring the angle-of-attack corrections for the moment) $c_{\ell_{3D}} = c_{\ell_{2D}}/\cos \Lambda$. The lift coefficient is thus increased by the factor $(\cos \Lambda)^{-1}$, with the restriction that the lift curve slope cannot exceed the unswept airfoil value c_{ℓ_α}. The equivalent angle of attack α_{equ} is the actual angle of attack corrected for unsteady potential flow effects (see refs. 6 and 7). The dynamic angle of attack α_{dyn} is a dynamic-stall correction of α, due to the pitch rate $\dot{\alpha}$:

$$\alpha_{\mathrm{dyn}} = \alpha - k \sqrt{\left| \frac{\dot{\alpha} c}{2V} \right|} \operatorname{sgn}(\dot{\alpha})$$

The additional subscript L or M on α_{dyn} indicates whether the correction is for the lift or for the moment. The difference is in the constant k, which for the NACA 0012 airfoil section is (k in degrees):

lift stall	$k = \max(0, \min(98, 124 - 161M))$
moment stall	$k = \max(0, \min(64, 98 - 171M))$

APPENDIX B

ROTOR CHARACTERISTICS, OPERATING CONDITIONS, AND CALCULATION PARAMETERS

Rotor Physical Description

Articulated blade with flap, lag, and feather hinges at hinge offset e; no precone, prelag, pitch/flap coupling, pitch/lag coupling, flap hinge damper, or structural damping; spar centroid, aerodynamic center, center-of-gravity, and elastic axis at quarter chord.

Geometry	
radius, R	7.62 m (25 ft)
number of blades, N	3
hinge offset, e/R	0.04
linear twist, from center of rotation to tip	$-10°$
chord, c	0.558 m
solidity, σ	0.070
Inertial and structural parameters	
running mass, m	11.97 kg/m
blade weight, M_b	859 N
first mass moment, S_b	320 kg-m
second mass moment, I_b	159 kg-m^2
Lock number, γ	8.43
flatwise bending stiffness, EI_{flat}	8.61×10^4 N-m^2
edgewise bending stiffness, EI_{edge}	1.148×10^6 N-m^2
torsional moment of inertia, I_θ	.004 kg-m^2/m
torsional strength, GJ	8.61×10^4 N-m^2

Three flatwise modes (rigid flapping and two elastic bending modes), two edgewise modes (rigid lag and one elastic bending mode), and one torsion mode (elastic torsion, with a rigid control system) used in the calculation of the blade motion.

Rotating natural frequencies of blade modes (per rev)

Flatwise	Edgewise	Torsion
1.030	0.245	5.836
2.694	3.851	
5.055		

Aerodynamic properties	
section airfoil	NACA 0012
tip loss factor, B	0.97
root cutout	$0.15R$

Operating Conditions

Rotor operating stages	
forward velocity, V	148 knots
tip speed, ΩR	229 m/sec (750 fps)
shaft angle-of-attack, α_s	0
advance ratio, μ	0.333
advancing tip Mach number, $M_{1.0,90}$	0.895
Rotor force trim (target values)	
thrust, T	73,395 N (16,500 lb)
propulsive force, PF	8260 N (1857 lb)
side force, Y	0
helicopter parasite drag area, f	2.32 m^2 (25 ft^2)
rotor blade loading, C_T/σ	0.090

Calculation Parameters

Blade motion calculated by a harmonic analysis method.

azimuth increment	5°
number of harmonics	15
tolerance on blade mode amplitude and velocity, in test for convergence	0.001
number of blade segments (radial)	15

Iterate on $\theta_{.75}$, A_{1S}, and B_{1S} to trim rotor thrust, propulsive force, and side fo tolerances:

thrust	445 N
propulsive force	44 N
side force	44 N

REFERENCES

1. Carta, F. O.; and Niebanck, C. F.: Prediction of Rotor Instability at High Forward Speeds. Volume III, Stall Flutter. USAAVLABS TR 68-18C, February 1969.

2. Arcidiacono, F. J.; Carta, F. O.; Casellini, L. M.; and Elman, H. L.: Investigation of Helicopter Control Loads Induced by Stall Flutter. USAAVLABS TR 70-2, March 1970.

3. Ham, Norman D.; and Garelick, Melvin S.: Dynamic Stall Considerations in Helicopter Rotors. J. American Helicopter Society, vol. 13, no. 2, April 1968.

4. Johnson, Wayne: The Effect of Dynamic Stall on the Response and Airloading of Helicopter Rotor Blades. J. American Helicopter Society, vol. 14, no. 2, April, 1969.

5. Johnson, Wayne: The Response and Airloading of Helicopter Rotor Blades due to Dynamic Stall. Massachusetts Institute of Technology ASRL TR 130-1, May 1970.

6. Tarzanin, F. J., Jr.: Prediction of Control Loads due to Blade Stall. J. American Helicopter Society, vol. 17, no. 2, April 1972.

7. Gormont, Ronald E.: A Mathematical Model of Unsteady Aerodynamics and Radial Flow for Application to Helicopter Rotors. USAAMRDL TR 72-67, May 1973.

8. Ormiston, Robert A.: Comparison of Several Methods for Predicting Loads on a Hypothesized Helicopter Rotor, AHS/NASA Ames Specialists Meeting on Rotorcraft Dynamics. February 13–15, 1974.

9. Arcidiacono, Peter J.: Prediction of Rotor Instability at High Forward Speeds. Volume I: Steady Flight Differential Equations of Motion for a Flexible Helicopter Blade with Chordwise Mass Unbalance. USAAVLABS TR 68-18A, February 1969.

TABLE I.– PERFORMANCE AND TRIM DATA

	Case							Notes
	1B	1A	1	2	3	4	5	
	Rigid blade Uniform inflow	Uniform inflow	Linear aero.	Static stall	UARL stall	MIT stall	Boeing stall	
T	73253	73155	73226	73022	73386	73453	73475	Target: 73395
PF	8269	8256	8260	8287	8265	8300	8234	Target: 8260
Y	31	−9	13	13	18	−4	−36	Target. 0
C_T	.00627	.00626	.00627	.00625	.00628	.00629	.00629	Target: .0063
C_T/σ	.0897	.0896	.0897	.0894	.0899	.0899	.0900	Target: .090
C_X/σ	.0101	.0101	.0101	.0101	.0101	.0102	.0101	Target: .0101
Q	34287	34069	37040	126403	59860	62199	64563	
C_Q	.000385	.000383	.000416	.001420	.000672	.000699	.000725	
C_Q/σ	.00551	.00547	.00595	.02031	.00962	.01000	.01038	
M_x	−2611	−1143	−1780	−9004	−4157	−4203	−10173	
M_y	−24865	−23618	−22470	−1889	−17339	−17080	−22843	
M_{pitch}	18.2	15.6	18.3	−876.0	−248.8	−365.3	−303.4	(mean)
P	1379	1371	1490	5085	2408	2502	2598	
Rotor D_r	5244	5173	6343	41541	15333	16214	17219	$D_r = \frac{P}{V} - PF$

TABLE 1.– PERFORMANCE AND TRIM DATA – Continued

	Case							Notes
	1B	1A	1	2	3	4	5	
	Rigid blade Uniform inflow	Uniform inflow	Linear aero.	Static stall	UARL stall	MIT stall	Boeing stall	
$(L/D)_r$	14.0	14.1	11.5	1.8	4.8	4.5	4.3	
equiv f	1.48	1.46	1.78	11.68	4.31	4.56	4.84	$f = D_r/q$
NC_{Q_O}/σ	.0012	.0012	.0012	.0362	.0105	.0125	.0148	lower stall limit = 0.0040 upper stall limit = 0.0080
β_O	4.49	4.45	4.44	4.38	4.54	4.48	4.38	
β_{1C}	7.76	7.64	7.24	1.43	5.82	6.00	6.19	$\beta_{1C} = \alpha_{TPP}$
β_{1S}	−.64	−.23	−.48	−3.16	−.61	−1.53	−2.43	
ζ_O	7.22	7.15	7.73	26.08	12.37	12.90	13.47	at root
$\theta_{.75}$	11.91	12.45	12.69	20.18	13.29	13.83	13.86	
A_{1S}	−3.39	−1.73	−2.15	−9.52	−4.79	−3.28	−4.33	
B_{1S}	14.64	14.71	14.95	19.04	14.99	15.81	16.40	
$\beta_{1S_{NFP}}$	−6.88	−7.07	−7.71	−17.61	−9.17	−9.81	−10.21	$\beta_{1C_{NFP}} = \beta_{1C} - B_{1S}$
$\beta_{1S_{NFP}}$	−4.03	−1.94	−2.63	−12.68	−5.40	−4.81	−6.76	$\beta_{1S_{NFP}} = \beta_{1S} + A_{1S}$
Calculation time (relative)	.6	1.0	1.0	1.2	3.5	2.8	1.8	per trim cycle

TABLE 1.– PERFORMANCE AND TRIM DATA – Concluded

	Case							Notes
	1B	1A	1	2	3	4	5	
	Rigid blade Uniform inflow	Uniform inflow	Linear aero.	Static stall	UARL stall	MIT stall	Boeing stall	
Magnitude vertical shear at root								
3rd harmonic	569	1174	1939		1169	2433	1819	
6th harmonic	31	36	160		271	178	227	
Magnitude inplane shear at root (rotating frame)								
2nd harmonic	988	1223	916		601	1326	142	
4th harmonic	102	970	952		329	1036	1134	
5th harmonic	40	160	27		231	93	138	
7th harmonic	18	18	36		156	36	124	

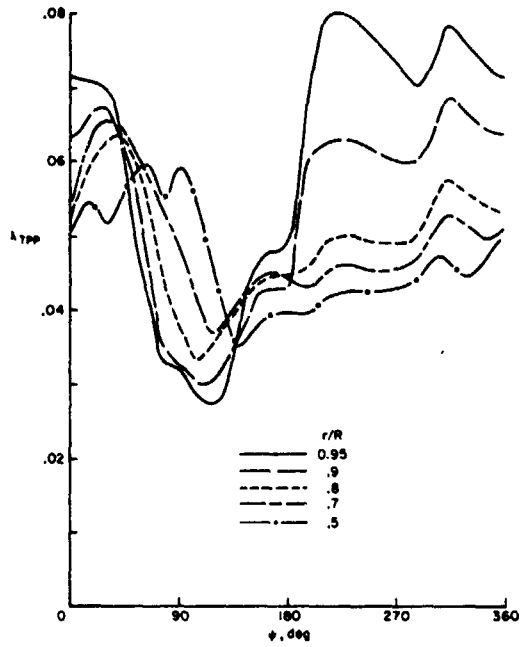

Figure 1.– Nonuniform wake-induced downwash used in the calculations.

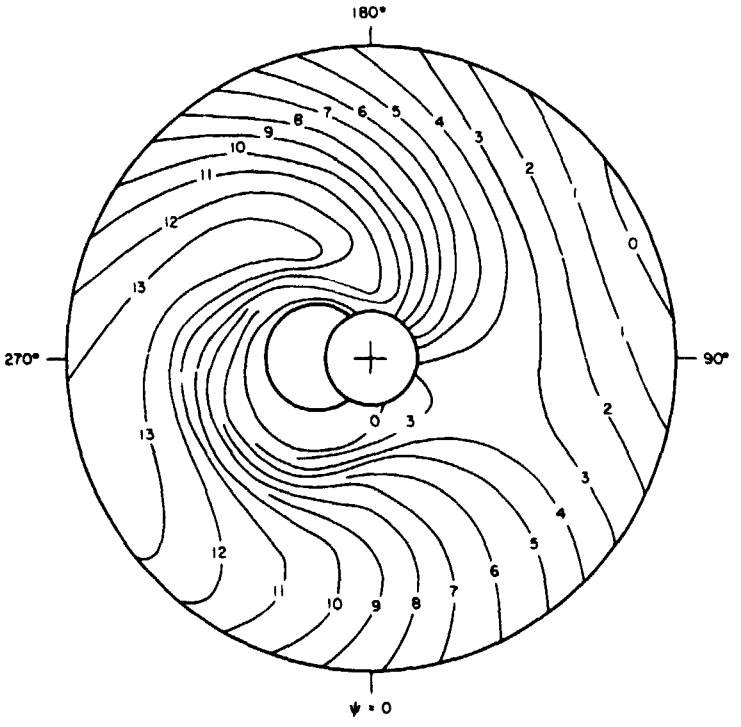

Figure 2.– Polar plot of angle-of-attack distribution (α, , for case 1A: uniform inflow.

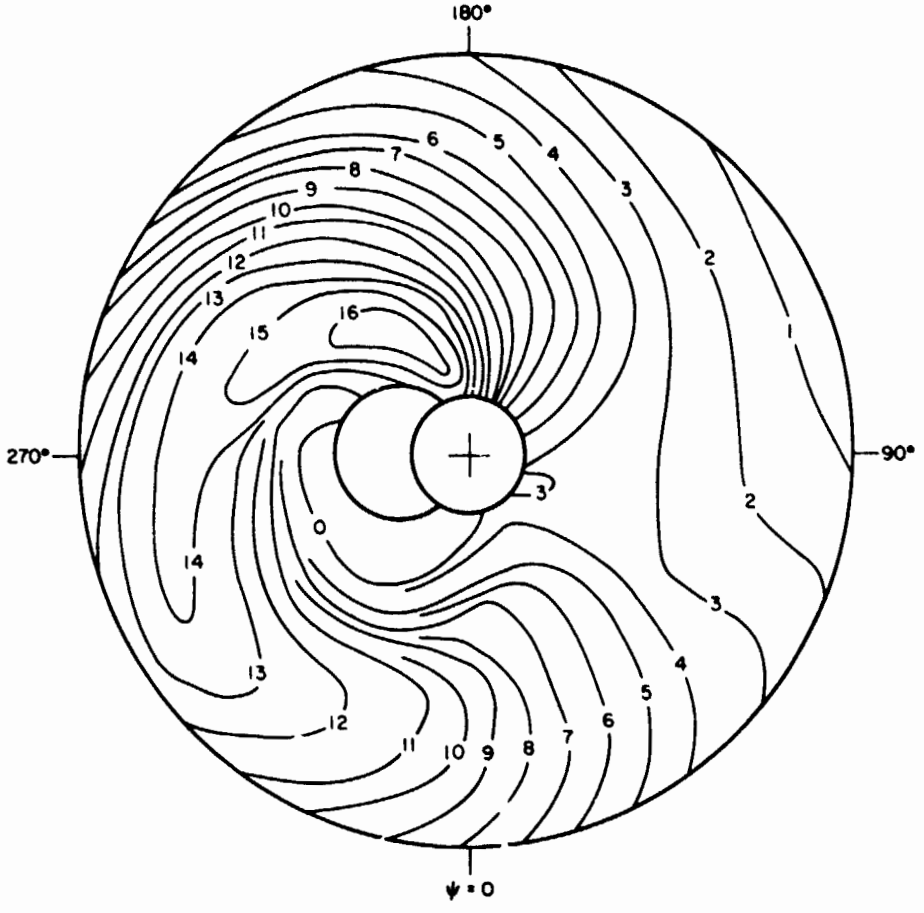

Figure 3.– Polar plot of angle-of-attack distribution (α, in degrees), for case 1: nonuniform inflow.

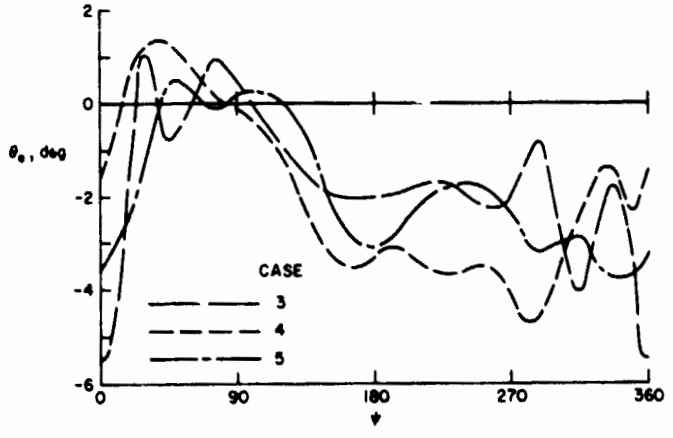

Figure 4.– Elastic torsion deflection at tip (proportional to root torsion moment since only one mode used: $M = \theta_e$ 322 N-m/deg).

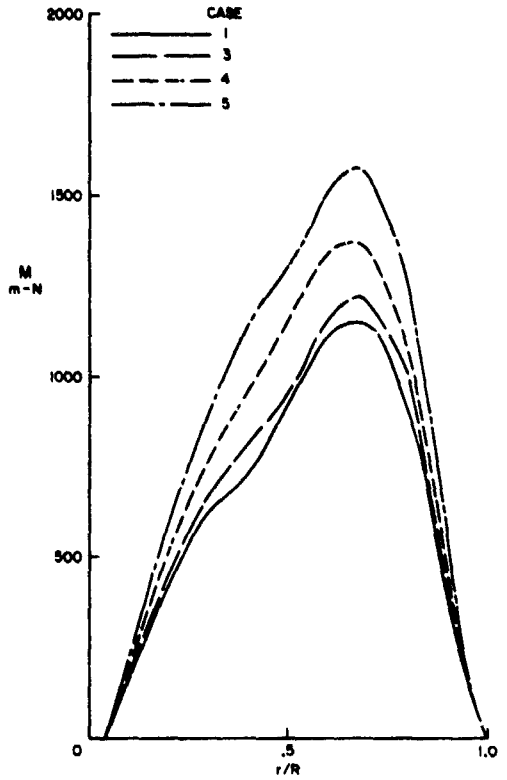

Figure 5.– One-half peak-to-peak flatwise blade bending moment.

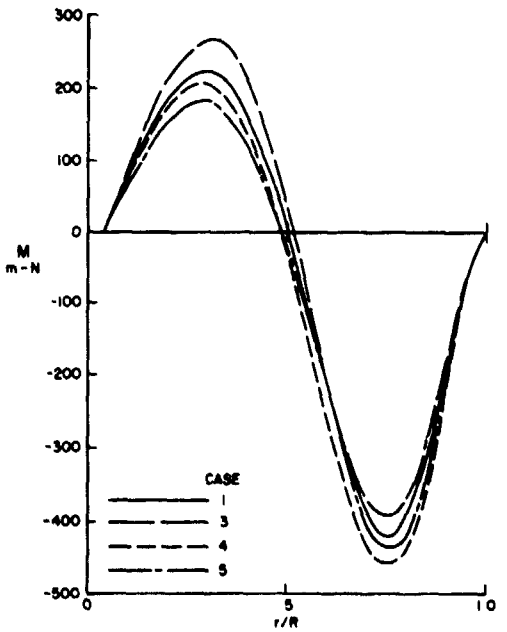

Figure 6.– Mean flatwise blade bending moment.

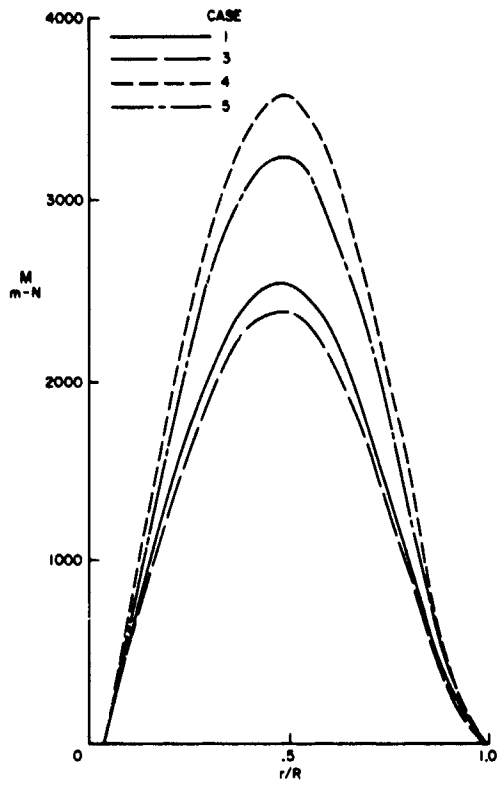

Figure 7.– One-half peak-to-peak edgewise blade bending moment.

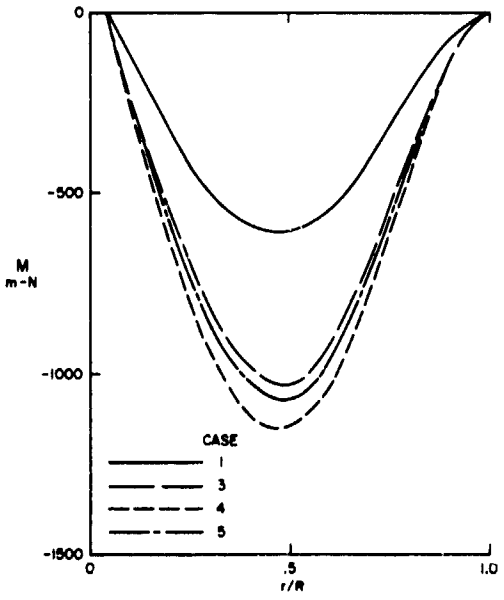

Figure 8.– Mean edgewise blade bending moment.

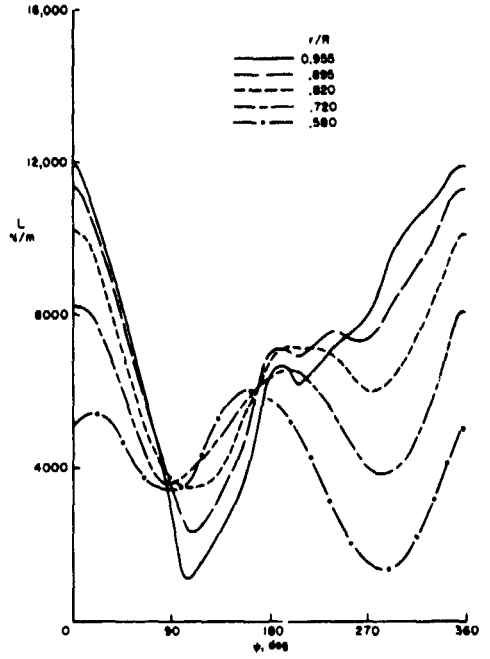

Figure 9.– Section aerodynamic lift force, case 1.

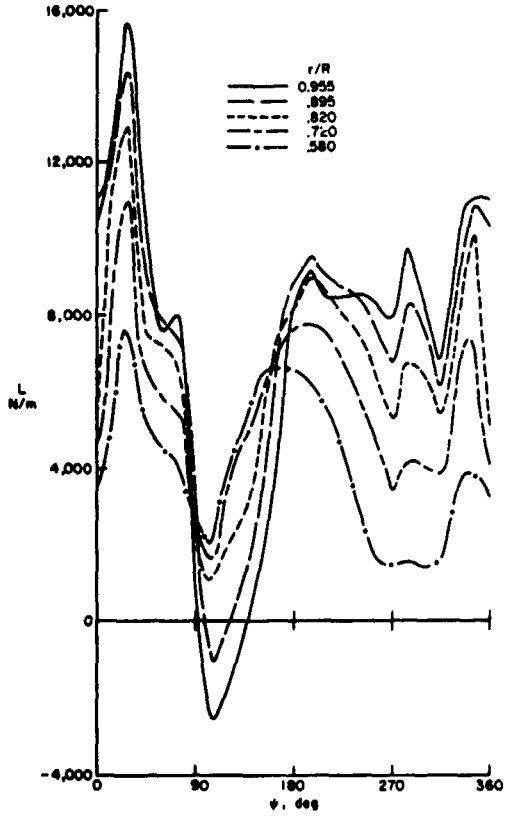

Figure 10.– Section aerodynamic lift force, case 3.

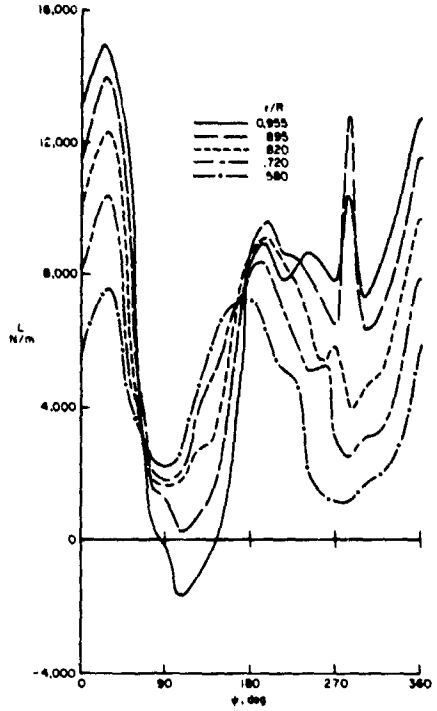

Figure 11.– Section aerodynamic lift force, case 4.

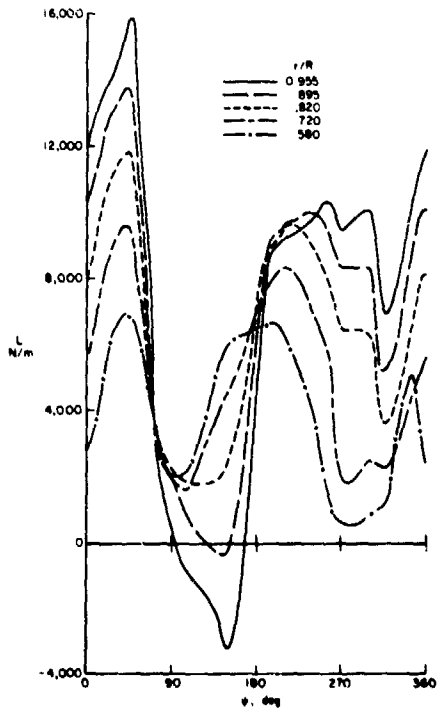

Figure 12.– Section aerodynamic lift force, case 5.

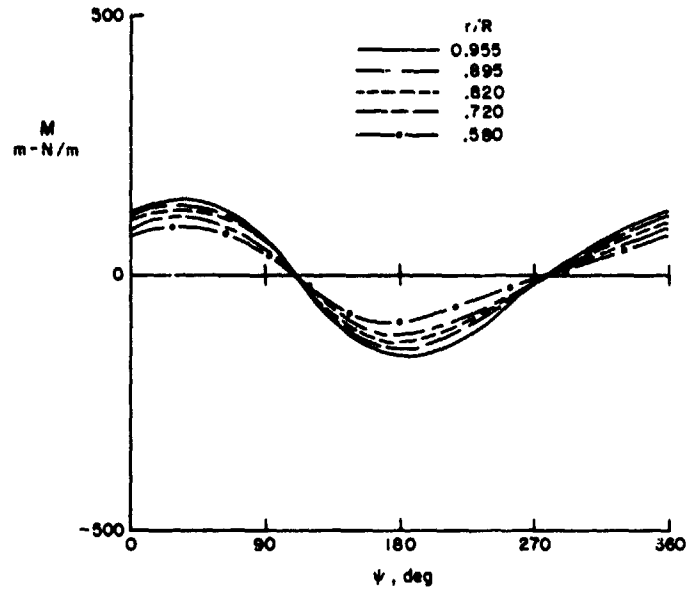

Figure 13.– Section aerodynamic pitching moment, case 1.

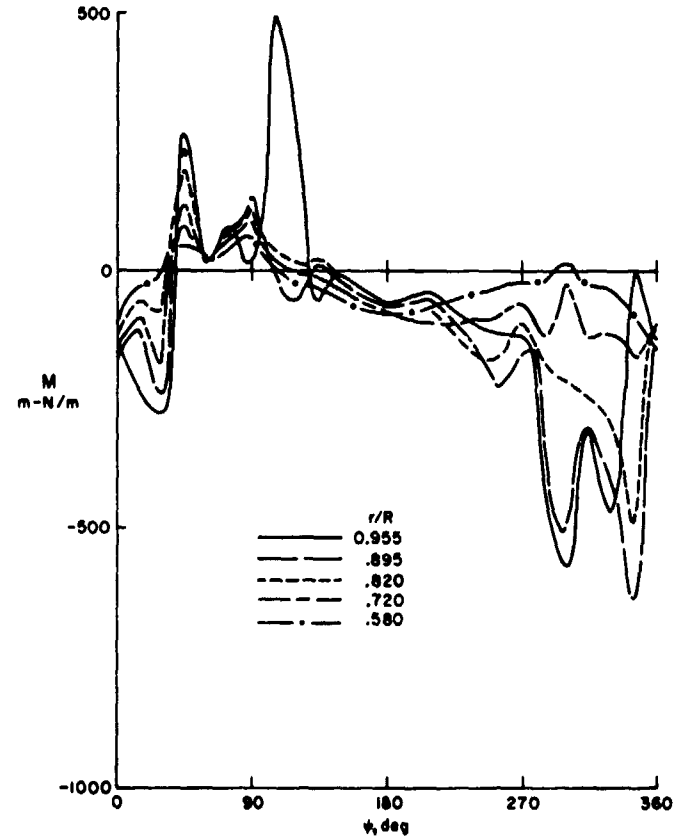

Figure 14.– Section aerodynamic pitching moment, case 3.

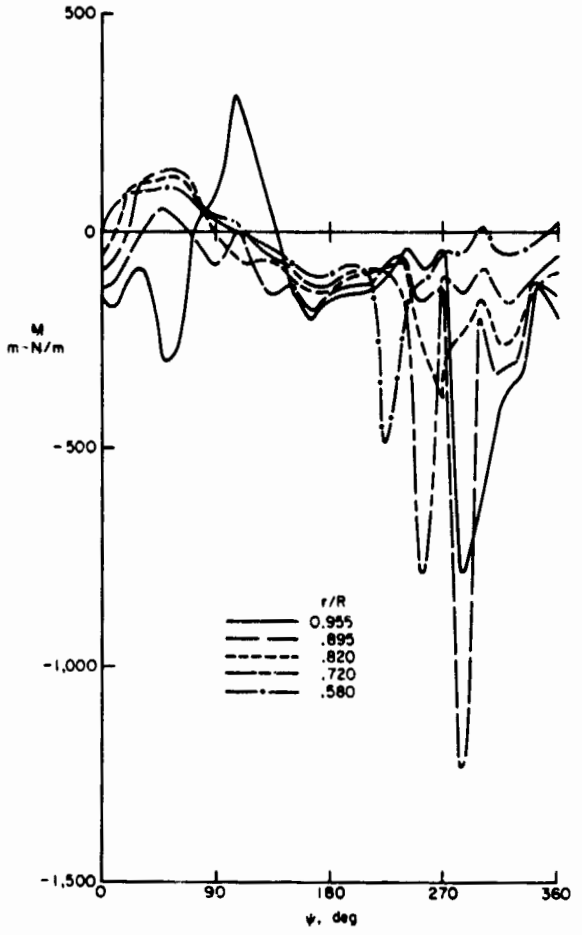

Figure 15.– Section aerodynamic pitching moment, case 4.

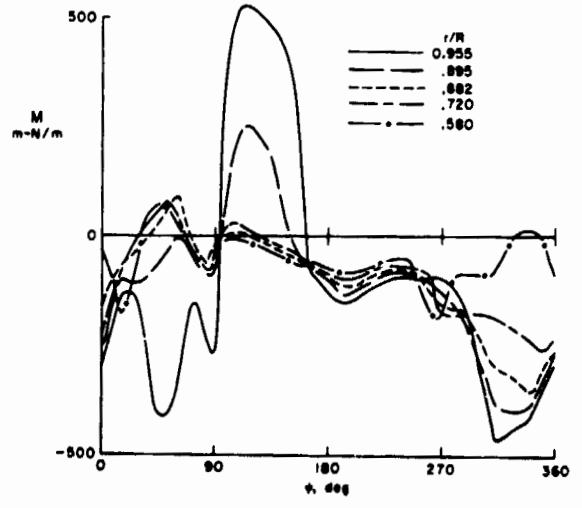

Figure 16.– Section aerodynamic pitching moment, case 5.

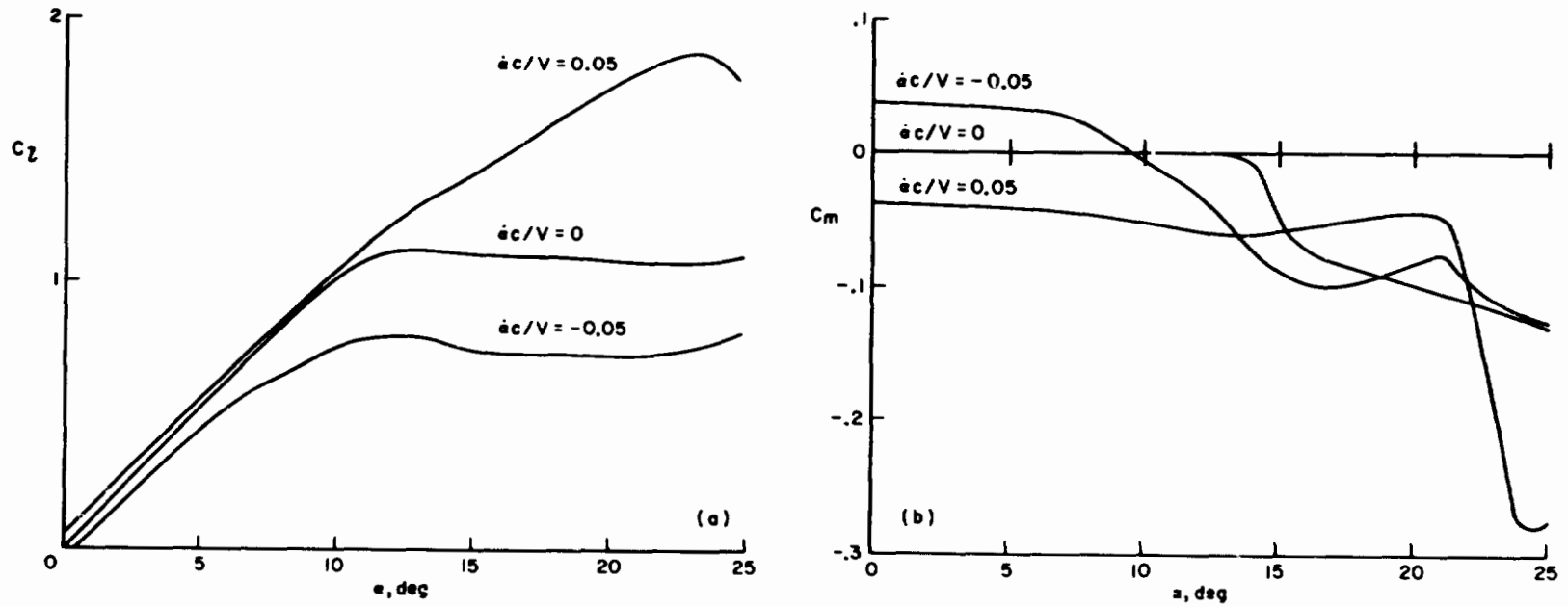

(a) Lift coefficient

(b) Moment coefficient

Figure 17.– UARL dynamic-stall method, typical results for lift and moment coefficients as function of α and $\dot{\alpha}$ (for $\ddot{\alpha} = 0$)